Nonperturbative model for wrinkling in highly bendable sheets

B. Davidovitch,[1] R. D. Schroll,[1,2] and E. Cerda[2]

[1]*Physics Department, University of Massachusetts, Amherst Massachusetts 01003, USA*
[2]*Departamento de Física, Universidad de Santiago, Av. Ecuador 3493, Santiago, Chile*

The wrinkled geometry of thin films is known to vary appreciably as the applied stresses exceed their buckling threshold. Here we derive and analyze a minimal, nonperturbative set of equations that captures the continuous evolution of radial wrinkles in the simplest axisymmetric geometry from threshold to the far-from-threshold limit, where the compressive stress collapses. This description of the growth of wrinkles is different from the traditional post-buckling approach and is expected to be valid for highly bendable sheets. Numerical analysis of our model predicts two surprising results. First, the number of wrinkles scales anomalously with the thickness of the sheet and the exerted load, in apparent contradiction with previous predictions. Second, there exists an invariant quantity that characterizes the mutual variation of the amplitude and number of wrinkles from threshold to the far-from-threshold regime.

I. INTRODUCTION

The wrinkling and buckling of elastic sheets are generally understood as perturbative phenomena. Near threshold (NT), where the compression along some direction is just enough to initiate buckling, traditional methods describe the shape by a perturbation of the Föppl–von Kármán (FvK) equations around the unstable, compressed state [1]. In contrast, the wrinkling state in very thin sheets, which support only negligible compressive stress before buckling, is described by a totally different perturbation theory. The basis of this far-from-threshold (FFT) expansion, which is the subject of tension field theory, is the singular "membrane limit" of sheets that support tension but not compression [2–4]. Since the critical loads diminish with thickness, the mechanics of wrinkled sheets and their transition from NT to FFT conditions are highly relevant for the study, control, miniaturization, and applicability of micro- and nanothickness films to new technologies.

The realization that wrinkling patterns are described by two distinct perturbation theories of FvK equations raises immediate problems. First, how does a wrinkling pattern transform from NT to FFT behavior when the control parameters (e.g., the sheet's thickness or the exerted loads) are smoothly varied? Another basic question pertains to the singular nature of the membrane limit, which may give rise to unphysical divergences in the FFT expansion that invalidate the computation of the wrinkle wavelength [5]. In this paper, we introduce a nonperturbative wrinkling model that is motivated by these problems and describes the transformation between the NT and FFT limits. The model projects the full FvK equations onto a set of nonlinear ordinary differential equations (ODEs). Focusing on an elementary axisymmetric stretching setup [Fig. 1(a)], we show that the model regularizes the FFT expansion and enables a complete quantitative description of wrinkling patterns.

The interest in the emerging sheet morphologies in axisymmetric setups, where sheets of circular shape are subjected to radial tensile loads, was triggered by a recent set of experiments [6–8]. The innovative use of capillary forces for stretching floating ultrathin sheets provided a natural playground for creating axisymmetric setups [7,8] and enabled an unprecedented precision in studying wrinkling phenomena. For a theorist, there is an obvious advantage in studying such setups. The radial stress is tensile, shear is negligible, and for a range of loading conditions the hoop (azimuthal) stress is compressive in some fraction of the sheet, hence the consequent buckling instability gives rise to a pattern of radial wrinkles. The simplest axisymmetric stretching setup is the Lamé geometry, Fig. 1(a) [1]: an annular sheet ($R_{in} \ll R_{out}$) under planar tensile loads (T_{in}, T_{out}, respectively). For the sake of simplicity, we will focus the current analysis on the Lamé setup. It is important to emphasize that the basic approach of this manuscript should be directly applicable for the study of wrinkles in other radial stretching geometries. Notable examples of such wrinkling patterns are the "sheet-on-drop" [9] and the "drop-on-sheet" [7,10] systems.

The high level of symmetry in this class of problems enabled the identification of dimensionless parameters that define the NT and FFT regimes: *confinement*, which depends on the tensile loads and governs the macroscopic extent of the compressive zone (or macrostructure), and *bendability*, which is inversely proportional to the bending modulus B and governs the wrinkle wavelength (or microstructure) [5]. For the Lamé problem, these parameters take the following specific form:

$$\text{confinement}: \tau = \frac{T_{in}}{T_{out}}; \quad \text{bendability}: \epsilon^{-1} = \frac{T_{out} R_{in}^2}{B}. \quad (1)$$

A schematic phase diagram (spanned by ϵ^{-1} and τ) of wrinkling patterns in the Lamé setup is depicted in Fig. 1(b) [5]. It shows that for a given ϵ, buckling occurs if $\tau > \tau_c(\epsilon)$, where the threshold curve $\tau_c(\epsilon) \to 2$ in the limit $\epsilon \to 0$, corresponding to highly bendable sheets. Close to (above) the threshold curve, the sheet exhibits an NT wrinkling state that is described as a perturbation around the compressed axisymmetric state. The NT regime in the (ϵ^{-1}, τ) plane narrows down for $\epsilon \ll 1$, where the sheet is so thin that it can support only a tiny compression. The FFT wrinkling state that prevails in the high-bendability regime ($\epsilon \ll 1$) is analyzed through a markedly different expansion of FvK equations, around the singular, compression-free membrane
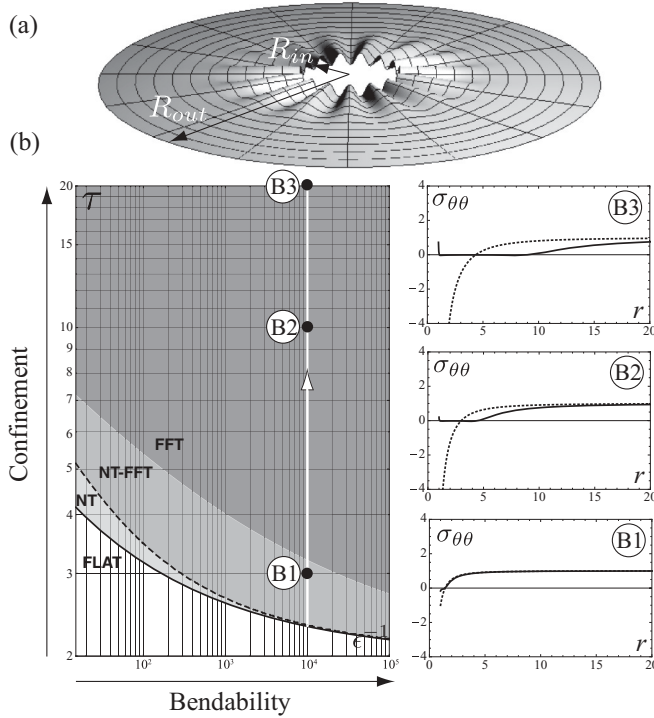
(a)

(b)

FIG. 1. (a) The Lamé set-up. (b) Left: The log-log phase diagram, spanned by the bendability (ϵ^{-1}) and confinement (τ) parameters, exhibits a flat region (white) that is bounded by the threshold $\tau_c(\epsilon)$ (solid curve), above which wrinkles are classified into NT (light gray), FFT (dark gray), and NT-FFT crossover regions. Right panels: The hoop stress at $\epsilon^{-1} = 10^4$ and $\tau = 3, 10, 20$ (solid lines). The dashed lines are the axisymmetric (Lamé) hoop stress for these values of τ.

limit, $\epsilon \to 0$, of sheets with vanishing bending modulus. These two analyses predict different scaling laws for the extent and number of wrinkles. By combining them into a single model we may unify the previous approaches for describing wrinkling phenomena [11–14].

The paper is organized as follows. In Sec. II we briefly review the distinct behaviors of wrinkles in the NT and FFT limits. In Sec. III we describe the nonperturbative model and show how it interpolates between the two limits and regularizes an unphysical singularity that baffled the original derivation of the FFT perturbation theory. In Sec. IV we describe our numerical analysis of the model equations and focus on two central findings: (1) an anomalous scaling of the number of wrinkles in the FFT limit and (2) an invariant quantity that characterizes the mutual variation of the amplitude and number of wrinkles between the NT and FFT limits. In Sec. V we conclude with some open questions and outlook. For the sake of clarity, we provide in Sec. III only heuristic arguments that explain the basic idea of the nonperturbative model and postpone to the appendices the technical derivation of the model from the complete FvK equations.

II. THE NEAR-THRESHOLD AND FAR-FROM-THRESHOLD LIMITS

The NT analysis is a linear stability analysis around the axisymmetric flat state, which is described by the classical

Lamé solution [1]. In the limit $R_{\text{out}} \gg R_{\text{in}}$ and for $\tau > 2$, the Lamé solution has a compressive hoop stress (i.e., $\sigma_{\theta\theta}(r) < 0$) in a zone $R_{\text{in}} < r < L_{\text{NT}} = R_{\text{in}}\sqrt{\tau - 1}$. To this state, an infinitesimal out-of-plane perturbation with a single wave number m is applied:

$$\zeta(r,\theta) = f(r)\cos(m\theta). \qquad (2)$$

As $\tau \to \tau_c(\epsilon)$, only a single critical mode $m_c(\epsilon)$ lowers the mechanical energy U_M relative to the axisymmetric state. U_M is the sum of the stretching and bending energies of the sheet, minus the external work done on the system due by the constant-tension boundary conditions. Since wrinkling is an infinitesimal perturbation, the extent of the wrinkled zone, defined as the distance from the tip of the wrinkles to the center, is approximated by L_{NT} of the Lamé axisymmetric solution.

In contrast, the FFT analysis begins with solving for the stress in the membrane limit by imposing $\sigma_{\theta\theta} = 0$ in a region $R_{\text{in}} < r < L$ with finite-amplitude wrinkles and an arbitrary L. Minimization of the dominant in-plane stretching energy over L yields the wrinkle extent $L_{\text{FFT}} = R_{\text{in}}\tau/2 > L_{\text{NT}}$. As the dominant energy depends only on the mere existence of the wrinkles and not on their number, the wrinkle number must be found by minimizing a *subdominant* energy that consists of bending and out-of-plane stretching. This subdominant energy is naturally minimized by a single mode with a wave number m_{FFT} (see Appendix D), a result supported by experiments [7]. In Ref. [5] the ratio between the subdominant and dominant energies was assumed to be $O(\epsilon^{1/2})$, an assumption which implies the scaling $m_{\text{FFT}} \sim \epsilon^{-1/4}$. However, the singular nature of the membrane limit complicates the calculation of m_{FFT}. The restriction that $\sigma_{\theta\theta} \to 0$ creates a "slaving" condition on the wrinkle amplitude $f(r)$:

$$\frac{1}{4}f(r)^2 m^2 = \frac{R_{\text{in}} T_{\text{out}}}{Y}\tau\, r \ln\left[\frac{\tau R_{\text{in}}}{2r}\right], \qquad (3)$$

where Y is the two-dimensional Young's modulus. The profile specified by Eq. (3) contains a cusp at $r = L_{\text{FFT}}$, which causes a divergence in the subdominant out-of-plane stretching energy [whose areal density is proportional to $(df/dr)^2$]. A central contribution of the current paper is a regularization of this singularity.

III. THE MODEL

In the following we describe our nonperturbative model and demonstrate that it captures the wrinkling behavior in both the NT and FFT limits. This model assumes that the wrinkling pattern is characterized by an out-of-plane deformation of the form (2) and a corresponding strain field ε_{ij} that is dominated by its axisymmetric (θ-independent) sector [see Eqs. (4c)]. This assumption is motivated by its applicability to both NT and FFT limits, but in the Appendices we demonstrate the self-consistency of this model. In the NT regime, m will correspond to the *single* unstable mode $m_c(\epsilon)$, while in the FFT regime it will be the *most* unstable (lowest energy) mode m_{FFT}. Thus, our model will track the variation of the most unstable mode between the NT and FFT limits. Equation (2) distinguishes our model from the traditional approach, which assumes that the post-buckling state couples an increasing number of unstable modes. In contrast to our model, which addresses the high

bendability regime $\epsilon^{-1} \gg 1$, the classical approach does not account for the collapse of compression and the consequent separation of energy scales; hence we expect it to be applicable only for low bendability values.

Assuming Eq. (2) with some arbitrary m and the domination of the stretching energy by the axisymmetric strain, the nonlinear FvK equations reduce to a set of ODEs for the normal and radial displacements, $f(r)$ and $u_r(r)$, respectively. Force balance in the radial direction gives

$$0 = \frac{1}{r}\partial_r(r\sigma_{rr}) - \sigma_{\theta\theta}/r, \qquad (4a)$$

where the stresses satisfy the linear (Hookean) response:

$$\sigma_{rr} = \frac{Y}{1-\nu^2}(\varepsilon_{rr} + \nu\varepsilon_{\theta\theta}); \quad \sigma_{\theta\theta} = \frac{Y}{1-\nu^2}(\varepsilon_{\theta\theta} + \nu\varepsilon_{rr}). \tag{4b}$$

and the strains are connected to the displacements through the *effective axisymmetric* relation:

$$\varepsilon_{rr} = \frac{du_r}{dr} + \frac{1}{4}\left(\frac{df}{dr}\right)^2; \quad \varepsilon_{\theta\theta} = \frac{u_r}{r} + \frac{1}{4}m^2\frac{f^2}{r^2} \tag{4c}$$

(and $\varepsilon_{r\theta} = 0$). The normal force balance equation is

$$B\nabla^4 f = \sigma_{rr}\frac{d^2 f}{dr^2} + \sigma_{\theta\theta}\left(\frac{1}{r}\frac{d}{dr} - \frac{m^2}{r^2}\right)f, \tag{4d}$$

where $\nabla^2 \equiv (\frac{d^2}{dr^2} + \frac{1}{r}\frac{d}{dr} - \frac{m^2}{r^2})$. In Appendices A and B, we present a detailed derivation of Eqs. (4), and in Appendix C we show that they conform to a variational system that satisfies $\delta U_M = 0$ and derive the boundary conditions.

Both NT and FFT results can be derived from analysis of Eqs. (4). The NT analysis of these equations yields identical results to the analogous buckling analysis of the full FvK equations. Dropping the nonlinear terms in Eqs. (4c) decouples the in-plane problem (4a)—(4c) from the out-of-plane problem (4d). This in-plane problem yields the Lamé solution. Using these stresses, the analysis of Eq. (4d) gives the standard buckling analysis of thin plates [14].

The slaving condition (3) and other features of the FFT regime can also be obtained from Eqs. (4a)–(4c). In the FFT analysis of Ref. [5], the contribution $\frac{1}{4}(df/dr)^2$ was omitted from the radial strain ε_{rr} in Eq. (4c). This reflected a pointwise matching between the compression-free wrinkled zone of $r > L_{\text{FFT}}$ and the wrinkled zone, $r < L_{\text{FFT}}$. Briefly, the vanishing hoop stress gives $\sigma_{\theta\theta} = 0 = \varepsilon_{\theta\theta} + \nu\varepsilon_{rr} = (u_r/r + f^2m^2/4r^2) + \nu du_r/dr$. We obtain Eq. (3) when the radial stress $\sigma_{rr} = T_{\text{in}}R_{\text{in}}/r$ is used to obtain u_r from the uniaxial relation $\sigma_{rr} = Y du_r/dr$ [compatible with a collapsed stress and the radial force balance Eq. (4a)]. This calculation predicts a cusp ($|df/dr| \to \infty$) at $r = L_{\text{FFT}}$. Our numerical results, below, show that this spurious divergence is related to the neglected term $\frac{1}{4}(df/dr)^2$. This term becomes important at the vicinity of the wrinkle tip, $r = L_{\text{FFT}}$, and its inclusion is shown to smooth out the cusp and hence regularize the energy calculation.

IV. RESULTS

Since the set of nonlinear equations (4) describes wrinkling in both NT and FFT limits, we propose its validity in the whole

high bendability regime $\epsilon^{-1} \gg 1$. Specifically, we explore wrinkling patterns by numerically solving Eqs. (4) for a range of numbers m along vertical (fixed ϵ) and horizontal (fixed τ) trajectories in the parameter space (ϵ^{-1}, τ). Our numerical analysis rapidly converges to the limit $R_{\text{out}} \to \infty$ when the ratio $R_{\text{out}}/R_{\text{in}} \approx 10^2$ or larger, so that we use a safe value of $R_{\text{out}}/R_{\text{in}} = 2 \times 10^2$. Additionally, since most of the experiments on wrinkling have been made on polymer membranes [7,8], we take the value $\nu = 1/3$ in our numerics.

As one moves away from threshold, $\tau_c(\epsilon)$, the axisymmetric state becomes unstable to a growing number of wrinkling modes (each corresponds to a different m). Our calculation shows that at each point (ϵ^{-1}, τ) the energy is minimized by a single value of wrinkle number $m_* = m_*(\epsilon, \tau)$.

Moving along fixed bendability lines [verticals in Fig. 1(b)], we observe that the stress recovers the Lamé solution when $\tau \gtrsim \tau_c(\epsilon)$. As τ increases, the stress varies appreciably and evolves into a shape that consists of a large region in which the compressive (negative) hoop component almost vanishes [Fig. 1(b)]. The distinctive collapse of the hoop stress signifies the emergence of the FFT regime. As far as we know, our model is the first one that captures the gradual transition of wrinkling patterns from threshold to the FFT regime assumed by tension field theory.

Since the FFT analysis predicts a wrinkle extent larger than that of the NT analysis, we expect a variation between these two limits with τ. Figure 2(a) shows the evolution of the extent $L_* = L_*(\epsilon, \tau)$ of the compressive region along the vertical (fixed-ϵ) paths. As expected, L_* is observed to increase monotonically with τ, approaching the predicted value $L_{\text{NT}}(\tau)$
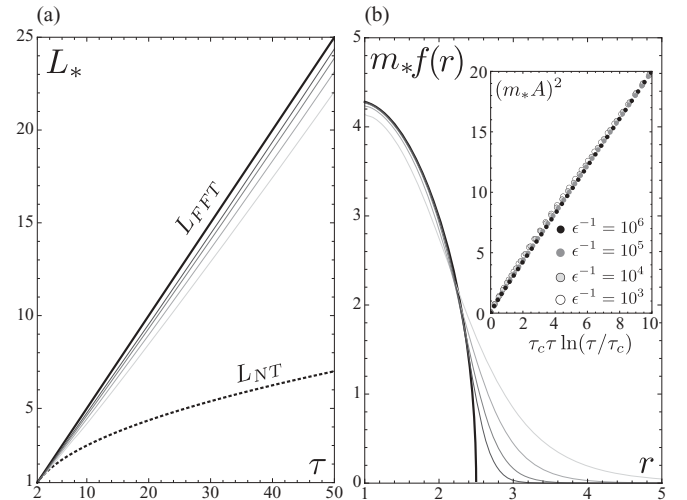

FIG. 2. (a) The computed extent $L_*(\epsilon, \tau)$ of the compressive region (where $\sigma_{\theta\theta} < 0$), plotted here as a function of τ, for several values of ϵ, increases with τ and appears to be bounded by the FFT prediction (upper solid black line) and the NT (Lamé) prediction (lower dashed line). (b) Computed wrinkle profiles $m_* f(r)$ (gray lines) for $\tau = 5$ and several values of ϵ, compared with the prediction of the FFT expansion, Eq. (3) (solid black line). (Inset) The amplitude for several values of ϵ follows the fit suggested by Eq. (5). In the figures L_* and r are re-scaled by R_{in}, and the amplitudes are scaled by $\sqrt{R_{\text{in}}^2 T_{\text{out}}/Y}$. The bendability values $\epsilon^{-1} = 10^3, 10^4, 10^5, 10^6$ are indicated with increasing intensity of gray.
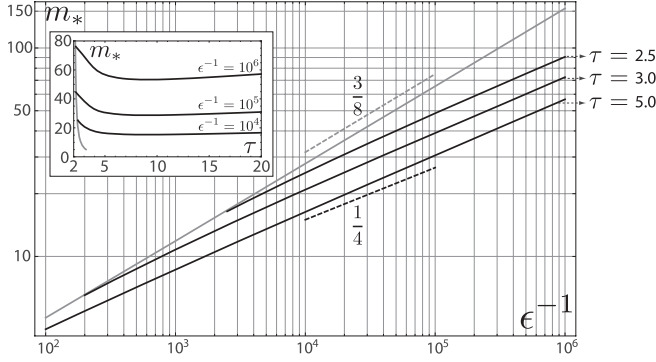
FIG. 3. Log-log plot of the number of wrinkles $m_*(\epsilon,\tau)$ as a function of ϵ^{-1}. The upper gray solid line is the threshold value $m_c(\epsilon)$, and the solid black lines describe $m_*(\epsilon,\tau)$ for several confinement values $\tau = 2.5, 3, 5$. The slopes shown were predicted in Ref. [5] by scaling arguments for the wrinkle number in the NT (upper dashed line) and FFT (lower dashed line). The inset shows $m_*(\epsilon,\tau)$ as a function of τ for different values of the bendability. The gray line corresponds to $m_c(\tau)$ after inverting the relation $\tau_c(\epsilon)$.

only for $\tau \to \tau_c(\epsilon)$, and converging to the predicted $L_{\mathrm{FFT}}(\tau)$, away from $\tau_c(\epsilon)$, when bendability is increased. Figure 2(b) shows that above threshold and for $\epsilon \ll 1$, the computed wrinkle profile $f(r)$ agrees with Eq. (3) in the "bulk" of the wrinkled region, but exhibits a substantial deviation from this prediction in a narrow layer between the wrinkled and unwrinkled zones. The width of the matching zone decreases as $\epsilon \to 0$. In this region, the large radial slope means that the radial strain term $(df/dr)^2$ in ε_{rr} is important and is balanced by an appropriate variation of the in-plane component du_r/dr from its compression-free value. This term regularizes the spurious divergence in the subdominant energy of the FFT analysis, and as such it is essential to the selection of the FFT pattern.

Figure 3 (inset) shows the variation of the wrinkle number $m_*(\epsilon,\tau)$ along few vertical, fixed-ϵ paths. As the confinement τ is increased from threshold, the wrinkle number is observed to decrease from the threshold value $m_c(\epsilon) = m_*[\epsilon,\tau_c(\epsilon)]$. This effect is elucidated in Fig. 3, where we plot $m_*(\epsilon,\tau)$ along two types of trajectories: the threshold curve $[\epsilon^{-1}, \tau = \tau_c(\epsilon)]$ and a fixed confinement line $(\epsilon^{-1}, \tau = \tau_0)$. The scaling of $m_c(\epsilon)$ as $\epsilon \to 0$ is in excellent agreement with the predicted NT scaling law [5,14]. For $m_*(\epsilon,\tau)$ we find the scaling $m_*(\epsilon,\tau) = k(\tau)\epsilon^{-\beta}$ with $\beta \approx 0.27$ and $k(\tau)$ a function of τ.

The surprise that comes with this finding stems from its apparent contradiction with the force balance argument in Refs. [5,12,13] that yields the scaling $m_{\mathrm{FFT}} \sim \epsilon^{-1/4}$. (Note, though, that our numerical analysis does not rule out the scaling $m_* \sim [\epsilon \log(1/\epsilon)]^{-1/4}$.) Notably, Ref. [5] assumed that the pattern is described by the compression-free profile, Eq. (3), and ignored the unphysical energetic divergence implied by this assumption [5]. The observation of the "anomalous" exponent $\beta > 1/4$ indicates that part of the subdominant energy becomes focused at the narrow matching zone, thus modifying the proposed dimensional scaling $\beta = 1/4$.

Another unexpected result comes from the wrinkle amplitude, defined here as $A(\epsilon,\tau) \equiv f(r = R_{\mathrm{in}})$. In the FFT regime, it is determined by the slaving condition (3). In the NT regime,

the amplitude must be proportional to $\sqrt{\tau - \tau_c(\epsilon)}$, thanks to the universal behavior of supercritical bifurcations [15]. Remarkably, we find that the amplitude is well approximated in both regimes by

$$A(\epsilon,\tau) \approx \sqrt{\frac{R_{\mathrm{in}}^2 T_{\mathrm{out}}}{Y}} \frac{\sqrt{2\tau\,\tau_c(\epsilon)}}{m_*(\epsilon,\tau)} \sqrt{\ln \frac{\tau}{\tau_c(\epsilon)}}. \qquad (5)$$

Note that this reduces to Eq. (3) for $\epsilon \to 0$, where $\tau_c(\epsilon) \approx 2$, and gives the expected square-root behavior for $\tau \approx \tau_c(\epsilon)$. As demonstrated in Fig. 2(b) (inset), this approximation is good throughout the parameter space, and thus it reflects an invariant property of the wrinkling pattern, valid in the NT and FFT limits as well as the intermediate regime connecting them.

V. SUMMARY

We have studied here a simple, nonperturbative model that captures the transition between the NT and FFT limits of wrinkling patterns in highly bendable sheets ($\epsilon \ll 1$). Our model proposes that this transition occurs through a single-mode pattern, Eq. (2), where the profile $f(r)$ and the number m of wrinkles vary smoothly between the two limits. Numerical analysis of this model shows that it regularizes the spurious singularity that hampered a former, crude version of the FFT expansion that assumed a pointwise matching between the wrinkled and unwrinkled parts of the sheet [5]. The single-mode assumption is supported by experimental observations [6,7,9] and by heuristic arguments (Appendix D), suggesting its validity under the free BCs assumed in this paper. Under other BCs, such as clamping at the boundary $r = R_{\mathrm{in}}$, the single-mode assumption is expected to fail, giving rise to a multimode cascade of wrinkles near the boundary. Let us note that despite these plausible considerations we are unaware of an analytic proof to the validity of the single-mode assumption, and a recent work, based on variational considerations, proposed that the actual energy minimizer could be a multimode wrinkling cascade (even under free BCs) [16]. A generalization of our model to multimode wrinkling patterns [i.e., replacing Eq. (2) by $\zeta(r,\theta) = \sum f_m(r)\cos(m\theta)$], may help to address this question, as well as other problems concerning the effect of various types of boundary conditions on the emerging wrinkling pattern.

The Lamé setup that is the focus of this paper provides the simplest extension of the classical Euler buckling instability from one-dimensional to an axisymmetric, two-dimensional configuration in which a planar, radial tensile load gives rise to a pattern of radial wrinkles. We expect that similar nonperturbative models could be developed and analyzed for studying wrinkling patterns in more complicated radial stretching setups by following the methodology introduced in this paper. These setups include, in particular, the sheet-on-drop [9] and drop-on-sheet [7] experiments. These experiments exhibit fascinating patterns of wrinkles which may undergo a transition to crumpled shapes. A nonperturbative model, similar to the one introduced here, may be useful to study some properties of such transitions.

In addition to its generalizability to multimode wrinkling patterns and other radial stretching problems, our results open up new interesting problems: How can one characterize

the transition between the low bendability regime, where a regular perturbation theory around the compressed state should be applicable, to the high-bendability wrinkling behavior described in this paper? Are wrinkling patterns in generic two-dimensional setups characterized by anomalous scaling relations? We hope that the nonperturbative wrinkling model reported here and the interesting questions that it raises will inspire future studies to explore these and other questions.

APPENDIX A: THE SINGLE-MODE SOLUTION TO THE FvK EQUATIONS

The aim of this Appendix is to show how the large deflection, small slopes assumption implies the existence of a single mode solution to Föppl–von Kármán (FvK) equations for the axisymmetric stretching of an annular sheet. Specifically, we show that for every wrinkle number m, the FvK equations reduce to a set of four nonlinear, coupled ODEs, whose solution gives the profile (out-of-plane deformation) $f(r)$ and the associated in-plane deformation field. In Appendix B we will show that in the high bendability regime ($\epsilon \ll 1$) the set of four ODEs can be reduced to only two ODEs [Eqs. (4)].

The sheet is stretched by constant stresses T_i and T_o (abbreviation for T_{in} and T_{out}) at its inner and outer boundaries R_i and R_o (abbreviations for R_{in} and R_{out}), respectively. We assume a deformation of the form of Eq. (2):

$$\zeta(r,\theta) = f(r)\cos m\theta. \tag{A1}$$

We observe that the source of nonlinearity in the FvK equations is the quadratic terms in the strains. Deriving the strain tensor associated with the ansatz $\zeta(r,\theta)$, we find a radial part (referred to here as "axisymmetric") and an oscillating ("nonaxisymmetric") part. For example,

$$\varepsilon_{rr} = \frac{\partial u_r}{\partial r} + \frac{1}{2}\left(\frac{\partial \zeta}{\partial r}\right)^2 = \frac{\partial u_r}{\partial r} + \frac{1}{4}\left(\frac{df}{dr}\right)^2(1 + \cos 2m\theta).$$

All other strain components and the associated components of the stress tensor and the displacement vector have similar axisymmetric and nonaxisymmetric parts. We derive below the explicit expressions.

1. Föppl–von Kármán equations

The complete set of equations that we need to solve are [3,17]

$$0 = \frac{1}{r}\frac{\partial(r\sigma_{rr})}{\partial r} - \frac{\sigma_{\theta\theta}}{r} + \frac{1}{r}\frac{\partial \sigma_{r\theta}}{\partial \theta}, \tag{A2a}$$

$$0 = \frac{1}{r}\frac{\partial(r\sigma_{r\theta})}{\partial r} + \frac{\sigma_{r\theta}}{r} + \frac{1}{r}\frac{\partial \sigma_{\theta\theta}}{\partial \theta}, \tag{A2b}$$

$$B\nabla^4\zeta = \sigma_{rr}\frac{\partial^2 \zeta}{\partial r^2} + 2\sigma_{r\theta}\frac{\partial}{\partial r}\left(\frac{1}{r}\frac{\partial \zeta}{\partial \theta}\right) + \sigma_{\theta\theta}\left(\frac{1}{r}\frac{\partial \zeta}{\partial r} + \frac{1}{r^2}\frac{\partial^2 \zeta}{\partial \theta^2}\right). \tag{A2c}$$

These equations, as well as the stress-strain relations, Eqs. (A3), and the strain-displacement relations (A4) assume that the deflection is characterized by small slopes everywhere ($|\nabla f| \ll 1$) and that the strains in the sheet are small.

The stress and strain tensors are related through the Hookean relations:

$$\varepsilon_{rr} = (\sigma_{rr} - \nu\sigma_{\theta\theta})/Y, \tag{A3a}$$

$$\varepsilon_{\theta\theta} = (\sigma_{\theta\theta} - \nu\sigma_{rr})/Y, \tag{A3b}$$

$$\varepsilon_{r\theta} = (1 + \nu)\sigma_{r\theta}/Y, \tag{A3c}$$

where Y is the two-dimensional Young's modulus. Finally, the relations between strains and displacements are

$$\varepsilon_{rr} = \frac{\partial u_r}{\partial r} + \frac{1}{2}\left(\frac{\partial \zeta}{\partial r}\right)^2, \tag{A4a}$$

$$\varepsilon_{\theta\theta} = \frac{u_r}{r} + \frac{1}{r}\frac{\partial u_\theta}{\partial \theta} + \frac{1}{2r^2}\left(\frac{\partial \zeta}{\partial \theta}\right)^2, \tag{A4b}$$

$$\varepsilon_{r\theta} = \frac{1}{2r}\frac{\partial u_r}{\partial \theta} + \frac{1}{2}\frac{\partial u_\theta}{\partial r} - \frac{u_\theta}{2r} + \frac{1}{2r}\frac{\partial \zeta}{\partial \theta}\frac{\partial \zeta}{\partial r}. \tag{A4c}$$

2. Boundary conditions

We study the case of an annular membrane of radii R_i and R_o that is stretched by the forces (per unit length) T_i and T_o [see Fig. 1(a)] under free boundary conditions (BCs):

$$\sigma_{rr}|_{r=R_i} = T_i \quad \sigma_{rr}|_{r=R_o} = T_o \quad \sigma_{r\theta}|_{r=R_i, R_o} = 0, \tag{A5a}$$

$$B\left[r\nabla^2\zeta - (1-\nu)\left(\frac{\partial \zeta}{\partial r} + \frac{1}{r}\frac{\partial^2 \zeta}{\partial \theta^2}\right)\right]_{r=R_i, R_o} = 0, \tag{A5b}$$

$$B\left[r\frac{\partial}{\partial r}\nabla^2\zeta + (1-\nu)\frac{\partial^2}{\partial\theta\partial r}\left(\frac{1}{r}\frac{\partial \zeta}{\partial \theta}\right)\right]_{r=R_i, R_o}$$
$$- \sigma_{rr}r\frac{\partial \zeta}{\partial r}\bigg|_{r=R_i, R_o} = 0. \tag{A5c}$$

Notice that the meaning of "free BCs" here is the absence of any forces in direction normal to the sheet (thus ruling out, e.g., clamping of the boundaries). The part that depends on the radial stress in Eq. (A5c) is usually not included in classic textbooks of elasticity [3,17]. In Ref. [18], Timoshenko points out that BCs with free edges and in-plane applied loads must include that term (see p. 372).

In Appendix C, we show that this set of BCs can be derived from a variational analysis of the energy functional. This is similar to the way by which free BCs are obtained in Ref. [17].

3. Projection along the axisymmetric sector

A solution of the form (A1) implies

$$\frac{1}{2}\left(\frac{\partial \zeta}{\partial r}\right)^2 = \frac{1}{4}\left(\frac{df}{dr}\right)^2(1 + \cos 2m\theta).$$

Substituting this in the strain-displacement relations (A4), we find

$$\varepsilon_{rr} = \frac{\partial u_r}{\partial r} + \frac{1}{4}\left(\frac{df}{dr}\right)^2 (1 + \cos 2m\theta), \tag{A6a}$$

$$\varepsilon_{\theta\theta} = \frac{u_r}{r} + \frac{1}{r}\frac{\partial u_\theta}{\partial \theta} + \frac{m^2}{4}f^2(1 - \cos 2m\theta), \tag{A6b}$$

$$\varepsilon_{r\theta} = \frac{1}{2r}\frac{\partial u_r}{\partial \theta} + \frac{1}{2}\frac{\partial u_\theta}{\partial r} - \frac{u_\theta}{2r} - \frac{m}{4r}f\frac{df}{dr}\sin 2m\theta, \tag{A6c}$$

where the in-plane displacements u_r, u_θ are considered general functions of r and θ. Requiring that the whole displacement vector field solves the FvK equations (A2) implies the structure:

$$u_r(r,\theta) = u_r^{(0)}(r) + u_r^{(2m)}(r)\cos 2m\theta, \tag{A7a}$$

$$u_\theta(r,\theta) = u_\theta^{(0)}(r) + u_\theta^{(2m)}(r)\sin 2m\theta. \tag{A7b}$$

The linearity of the stress-strain relations in Eqs. (A3) and the linearity of the equations of equilibrium for the stresses, Eqs. (A2), show that a separation of the displacement field into axisymmetric and nonaxisymmetric components induces a similar separation for the stresses and the strains. Using Eqs. (A3), (A6), and (A7), we obtain the following structure of the stress components:

$$\sigma_{rr}(r,\theta) = \sigma_{rr}^{(0)}(r) + \sigma_{rr}^{(2m)}(r)\cos 2m\theta, \tag{A8a}$$

$$\sigma_{\theta\theta}(r,\theta) = \sigma_{\theta\theta}^{(0)}(r) + \sigma_{\theta\theta}^{(2m)}(r)\cos 2m\theta, \tag{A8b}$$

$$\sigma_{r\theta}(r,\theta) = \sigma_{r\theta}^{(0)}(r) + \sigma_{r\theta}^{(2m)}(r)\sin 2m\theta. \tag{A8c}$$

The shear term can be proven to be zero. Fourier integrating $\int_0^{2\pi} d\theta (\cdot)$ the two sides of Eq. (A2b), and using Eqs. (A3) and (A4), we find

$$0 = \frac{1}{r}\frac{d(r\sigma_{r\theta}^{(0)})}{dr} + \frac{\sigma_{r\theta}^{(0)}}{r}, \quad \sigma_{r\theta}^{(0)} = \frac{Y}{1+\nu}\left(\frac{1}{2}\frac{du_\theta^{(0)}}{dr} - \frac{u_\theta^{(0)}}{2r}\right).$$

The solution of the first equation gives $\sigma_{r\theta}^{(0)}(r) = A/r^2$. The boundary condition of zero shear at $r = R_i, R_o$ implies that $\sigma_{r\theta}^{(0)}(r) = 0$. Similarly, the second equation gives $u_\theta^{(0)}(r) = Br$, a rigid rotation of the system that can be fixed to zero. We conclude that $u_\theta^{(0)}(r) = 0$.

4. ODEs for the displacement field

Now we are at a position to reduce the FvK Eqs. (A2) into a set of four ODEs for the displacement functions $f(r)$, $u_r^{(0)}(r)$, $u_r^{(2m)}(r)$, and $u_\theta^{(2m)}(r)$. Substituting the ansatz (A1) and expressions (A8) into the normal force balance, Eq. (A2c), we obtain, after Fourier integrating both sides $\int_0^{2\pi} d\theta \cos(m\theta) (\cdot)$:

$$B\left(\frac{d^2}{dr^2} + \frac{1}{r}\frac{d}{dr} - \frac{m^2}{r^2}\right)^2 f$$
$$= \left[\sigma_{rr}^{(0)}(r) + \frac{1}{2}\sigma_{rr}^{(2m)}(r)\right]\frac{d^2 f}{dr^2} - m\sigma_{r\theta}^{(2m)}(r)\frac{d}{dr}\left(\frac{f}{r}\right)$$
$$+ \left[\sigma_{\theta\theta}^{(0)}(r) + \frac{1}{2}\sigma_{\theta\theta}^{(2m)}(r)\right]\left(\frac{1}{r}\frac{d}{dr} - \frac{m^2}{r^2}\right)f. \tag{A9a}$$

From the two other equilibrium Eqs. (A2a) and (A2b) we obtain, after Fourier integration $\int_0^{2\pi} d\theta (\cdot)$ and

$\int_0^{2\pi} d\theta \sin(2m\theta) (\cdot)$:

$$0 = \frac{1}{r}\frac{d(r\sigma_{rr}^{(0)})}{dr} - \frac{\sigma_{\theta\theta}^{(0)}}{r}, \tag{A9b}$$

$$0 = \frac{1}{r}\frac{d(r\sigma_{rr}^{(2m)})}{dr} - \frac{\sigma_{\theta\theta}^{(2m)}}{r} + \frac{2m}{r}\sigma_{r\theta}^{(2m)}, \tag{A9c}$$

$$0 = \frac{1}{r}\frac{d(r\sigma_{r\theta}^{(2m)})}{dr} + \frac{\sigma_{r\theta}^{(2m)}}{r} - \frac{2m}{r}\sigma_{\theta\theta}^{(2m)}. \tag{A9d}$$

The four equations (A9) can be expressed in terms of the four functions $f(r)$, $u_r^{(0)}(r)$, $u_r^{(2m)}(r)$, and $u_\theta^{(2m)}(r)$, by employing the stress-strain relations:

$$\varepsilon_{rr}^{(0)} = \left(\sigma_{rr}^{(0)} - \nu\sigma_{\theta\theta}^{(0)}\right)/Y, \tag{A10a}$$

$$\varepsilon_{\theta\theta}^{(0)} = \left(\sigma_{\theta\theta}^{(0)} - \nu\sigma_{rr}^{(0)}\right)/Y, \tag{A10b}$$

$$\varepsilon_{rr}^{(2m)} = \left(\sigma_{rr}^{(2m)} - \nu\sigma_{\theta\theta}^{(2m)}\right)/Y, \tag{A10c}$$

$$\varepsilon_{\theta\theta}^{(2m)} = \left(\sigma_{\theta\theta}^{(2m)} - \nu\sigma_{rr}^{(2m)}\right)/Y, \tag{A10d}$$

$$\varepsilon_{r\theta}^{(2m)} = (1 + \nu)\sigma_{r\theta}^{(2m)}/Y, \tag{A10e}$$

and the strain-displacement relations:

$$\varepsilon_{rr}^{(0)} = \frac{du_r^{(0)}}{dr} + \frac{1}{4}\left(\frac{df}{dr}\right)^2, \tag{A10f}$$

$$\varepsilon_{\theta\theta}^{(0)} = \frac{u_r^{(0)}}{r} + \frac{m^2}{4r^2}f^2, \tag{A10g}$$

$$\varepsilon_{rr}^{(2m)} = \frac{du_r^{(2m)}}{dr} + \frac{1}{4}\left(\frac{df}{dr}\right)^2, \tag{A10h}$$

$$\varepsilon_{\theta\theta}^{(2m)} = \frac{u_r^{(2m)}}{r} + \frac{2m}{r}u_\theta^{(2m)} - \frac{m^2}{4r^2}f^2, \tag{A10i}$$

$$\varepsilon_{r\theta}^{(2m)} = -\frac{m}{r}u_r^{(2m)} + \frac{1}{2}\frac{du_\theta^{(2m)}}{dr} - \frac{u_\theta^{(2m)}}{2r} - \frac{m}{4r}f\frac{df}{dr}. \tag{A10j}$$

With the aid of Eqs. (A10), Eqs. (A9) constitute a set of four equations for the four unknown functions $\{f(r), u_r^{(0)}(r), u_r^{(2m)}(r), u_\theta^{(2m)}(r)\}$, so that the system of equations is well posed [19].

APPENDIX B: REDUCING THE FvK EQUATIONS INTO THE NONPERTURBATIVE MODEL

Equations (A9) involve both the axisymmetric ($\sigma^{(0)}$) and nonaxisymmetric ($\sigma^{(2m)}$) modes of the stress. Note that these modes appear together only in (A9a). In this Appendix, we will show that the contribution of the $\sigma^{(2m)}$ terms to Eq. (A9a) is negligible in the high bendability regime ($\epsilon \ll 1$). This means that the four equations (A9) may be reduced to two equations for the functions $f(r)$ and $u_r^{(0)}(r)$.

Rearranging terms, the right-hand side of (A9) may be rewritten as

$$\sigma_{rr}^{(0)}\frac{d^2 f}{dr^2} + \sigma_{\theta\theta}^{(0)}\left(\frac{1}{r}\frac{d}{dr} - \frac{m^2}{r^2}\right)f + \frac{1}{2}\sigma_{rr}^{(2m)}\frac{d^2 f}{dr^2}$$
$$- m\sigma_{r\theta}^{(2m)}\frac{d}{dr}\left(\frac{f}{r}\right) + \frac{1}{2}\sigma_{\theta\theta}^{(2m)}\left(\frac{1}{r}\frac{d}{dr} - \frac{m^2}{r^2}\right)f. \tag{B1}$$

The relative size of the components of the $2m$ stress fields may be estimated from the stress balances of Eqs. (A9c) and (A9d). Approximating $1/r \sim d/dr \sim 1/R_i$, the latter implies

that $\sigma_{r\theta}^{(2m)} \sim m \, \sigma_{\theta\theta}^{(2m)}$. Assuming that $m \gg 1$, Eq. (A9c) means that

$$\sigma_{rr}^{(2m)} \sim m \, \sigma_{r\theta}^{(2m)} \sim m^2 \, \sigma_{\theta\theta}^{(2m)}.$$

In turn, this means that all of the $2m$ terms in Eq. (A9a) will be of the same order [20]. Thus, to be able to ignore them, we need only prove that $\sigma_{rr}^{(2m)}/\sigma_{rr}^{(0)} \ll 1$.

In order to estimate this ratio, we notice that the axisymmetric stress is induced by the stretching forces at the boundaries, and we estimate $\sigma_{rr}^{(0)} \sim T_i$. Note that the corresponding axisymmetric strain $\epsilon_{rr}^{(0)} \sim \sigma_{rr}^{(0)}/Y$ is dominated by the in-plane component $du_r^{(0)}/dr$ [see Eq. (A10f)], which remains finite even when the out-of-plane contribution $(df/dr)^2 = 0$ (i.e., below threshold). In contrast, the nonaxisymmetric stress $\sigma_{rr}^{(2m)}$ is not induced directly by the boundary forces (obviously, as $\sigma_{rr}^{(2m)} = 0$ below threshold). By Eq. (A10h), the in-plane contribution to the nonaxisymmetric strain $du_r^{(2m)}/dr$ must scale with the out-of-plane contribution $(df/dr)^2$. Thus, we may estimate the nonaxisummetric radial stress by $\sigma_{rr}^{(2m)} \sim Y\epsilon_{rr}^{(2m)} \sim Yf^2/R_i^2$. The condition for the negligibility of the second-order stress in Eq. (A9a) reduces to

$$m \gg 1 \quad \text{and} \quad \frac{Yf^2}{T_i R_i^2} \ll 1. \tag{B2}$$

From the "slaving" condition (3), we have $Yf^2/T_i R_i^2 \sim m^{-2} \ll 1$ when $m \gg 1$. From force balance, we expect $m \sim \epsilon^{-1/4}$ [5] (and find numerically that $m \sim \epsilon^{-0.27}$), so in the high bendability limit, ignoring the contribution from the second-order stress is a valid assumption [21].

1. The reduced model

The above argument shows that we may reduce Eqs. (A9) to two equations that involve only $f(r)$ and $u_r^{(0)}(r)$ (the super-index is henceforth dropped)

$$B\left(\frac{d^2}{dr^2} + \frac{1}{r}\frac{d}{dr} - \frac{m^2}{r^2}\right)^2 f = \sigma_{rr}\frac{d^2 f}{dr^2} + \sigma_{\theta\theta}\left(\frac{1}{r}\frac{d}{dr} - \frac{m^2}{r^2}\right)f, \tag{B3a}$$

$$0 = \frac{1}{r}\frac{d(r\sigma_{rr})}{dr} - \frac{\sigma_{\theta\theta}}{r}, \tag{B3b}$$

that must be solved with the stress-strain relations

$$\varepsilon_{rr} = (\sigma_{rr} - \nu\sigma_{\theta\theta})/Y, \tag{B3c}$$

$$\varepsilon_{\theta\theta} = (\sigma_{\theta\theta} - \nu\sigma_{rr})/Y, \tag{B3d}$$

and the strain-displacement relations

$$\varepsilon_{rr} = \frac{du_r}{dr} + \frac{1}{4}\left(\frac{df}{dr}\right)^2, \tag{B3e}$$

$$\varepsilon_{\theta\theta} = \frac{u_r}{r} + \frac{m^2}{4r^2}f^2. \tag{B3f}$$

Equations (B3) constitute the model used in our work.

2. BCs for the model

Since the BCs (A5) for the Lamé problem are linear, it is straightforward to obtain

$$\sigma_{rr}|_{r=R_i} = T_i \quad \sigma_{rr}|_{r=R_o} = T_o, \tag{B4a}$$

$$B\left[r\left(\nabla_r^2 - \frac{m^2}{r^2}\right)f - (1-\nu)\left(\frac{df}{dr} - m^2\frac{f}{r}\right)\right]_{r=R_i,\, R_o} = 0, \tag{B4b}$$

$$\left[B\left\{-r\frac{d}{dr}\left[\left(\nabla_r^2 - \frac{m^2}{r^2}\right)f\right] + (1-\nu)m^2\frac{d}{dr}\left(\frac{f}{r}\right)\right\}\right.$$
$$\left. + 2\pi\sigma_{rr}r\frac{df}{dr}\right]_{r=R_i,\, R_o} = 0. \tag{B4c}$$

This gives us a self-contained system describing a single-mode solution (with m wrinkles) for the out-of-plane displacement. This system can be solved for any m; the optimal value will be found by minimizing the mechanical energy of the system. This energy functional is derived in Appendix C.

APPENDIX C: VARIATIONAL ANALYSIS AND THE MECHANICAL ENERGY

The aim of this Appendix is to provide a variational principle for the Eqs. (B3) [or Eqs. (4)] and BCs (B4). We will show that there exists a functional that corresponds to the mechanical energy of the system. The mechanical energy is of fundamental importance in our framework since energy minimization provides a mechanism to select the number of wrinkles.

1. Bending energy

The bending energy in the small deflection approximation is [17]

$$U_B = \frac{B}{2}\int_A dA\,\{(\nabla^2\zeta)^2 - (1-\nu)[\zeta,\zeta]\}. \tag{C1}$$

Here,

$$\nabla^2\zeta = \left(\nabla_r^2 + \frac{1}{r^2}\frac{\partial^2}{\partial\theta^2}\right)\zeta,$$

$$[\zeta,\zeta] = 2\frac{\partial^2\zeta}{\partial r^2}\left(\frac{1}{r}\frac{\partial\zeta}{\partial r} + \frac{1}{r^2}\frac{\partial^2\zeta}{\partial\theta^2}\right) - 2\left(\frac{1}{r}\frac{\partial^2\zeta}{\partial r\partial\theta} - \frac{1}{r^2}\frac{\partial\zeta}{\partial\theta}\right)^2,$$

where we have defined $\nabla_r^2 \equiv \frac{1}{r}\frac{\partial}{\partial r}(r\frac{\partial}{\partial r})$. In the small deflection limit, $\nabla^2\zeta$ is the mean curvature and $[\zeta,\zeta]$ is twice the Gaussian curvature.

Using the ansatz (A1), we obtain

$$\nabla^2\zeta = \cos^2 m\theta\left(\nabla_r^2 - \frac{m^2}{r^2}\right)f,$$

$$[\zeta,\zeta] = \cos^2 m\theta \times 2\frac{d^2 f}{dr^2}\left(\frac{1}{r}\frac{df}{dr} - \frac{m^2}{r^2}f\right)$$
$$- \sin^2 m\theta \times 2m^2\left(\frac{1}{r}\frac{df}{dr} - \frac{1}{r^2}f\right)^2.$$

Substituting these relations into the energy and integrating gives the bending energy

$$U_B = \frac{2\pi}{2}\frac{B}{2}\int_{R_i}^{R_o} r\,dr\left[\left(\nabla_r^2 - \frac{m^2}{r^2}\right)f\right]^2 - \frac{2\pi}{2}B(1-\nu)\kappa|_{R_i}^{R_o},$$

where the factor $2\pi/2$ in front of the integral reflects the angular integration. The function

$$\kappa(r) \equiv \frac{1}{2}\left[\left(\frac{df}{dr}\right)^2 - m^2 \frac{d}{dr}\left(\frac{f^2}{r}\right)\right]$$

is simply the area integral of the Gaussian curvature [22].

2. Stretching energy

The in-plane elastic energy is [3,17]

$$U_S = \frac{Y}{2(1-\nu^2)}\int_A dA \left[\varepsilon_{rr}^2 + \varepsilon_{\theta\theta}^2 + 2\nu\varepsilon_{rr}\varepsilon_{\theta\theta} + 2(1-\nu)\varepsilon_{r\theta}^2\right].$$
$$(C2)$$

Here we use the displacement relations (A7) to the lowest order to obtain the strains and evaluate the energy

$$\varepsilon_{rr} = \frac{du_r^{(0)}}{dr} + \frac{1}{4}\left(\frac{df}{dr}\right)^2, \tag{C3a}$$

$$\varepsilon_{\theta\theta} = \frac{u_r^{(0)}}{r} + \frac{m^2}{4}f^2, \tag{C3b}$$

$$\varepsilon_{r\theta} = \frac{1}{2}\frac{du_\theta^{(0)}}{dr} - \frac{u_\theta^{(0)}}{2r}. \tag{C3c}$$

3. External work and mechanical energy

When forces T_i and T_o are applied to the boundaries, external work is done on the system. This work can be computed as

$$W^e = \int_{\mathcal{C}} dl\,\hat{n}_i\sigma_{ij}u_j = 2\pi T_o R_o u_r(R_o) - 2\pi T_i R_i u_r(R_i).$$

Here $\mathcal{C}$ is the contour line marking the boundary of the annular membrane. The deformation of the membrane due to these constant forces is obtained by minimizing the mechanical energy

$$U_M = U_B + U_S - W^e$$

for free variations of the displacement.

4. First variation

Enforcing $\delta U_M = 0$ for free variations of $u_r^{(0)}$, $u_r^{(2m)}$, $u_\theta^{(0)}$, $u_\theta^{(2m)}$, and f gives, after a straightforward but lengthy calculation [23], the system Eqs. (A9). Here we show that considering only variations in $u_r^{(0)}$, $u_\theta^{(0)}$, and f leads consistently to the reduced model (B3).

a. Bending energy

We apply manipulations, similarly to Ref. [17]. The variation of the first term is

$$\delta\frac{1}{2}\int_{R_i}^{R_o} r\,dr\left[\left(\nabla_r^2 - \frac{m^2}{r^2}\right)f\right]^2 = \int_{R_i}^{R_o} r\,dr\left[\left(\nabla_r^2 - \frac{m^2}{r^2}\right)f\right]\left[\left(\frac{d^2}{dr^2} + \frac{1}{r}\frac{d}{dr} - \frac{m^2}{r^2}\right)\delta f\right].$$

Successive integrations by parts give the expression

$$\delta\frac{1}{2}\int_{R_i}^{R_o} r\,dr\left[\left(\nabla_r^2 - \frac{m^2}{r^2}\right)f\right]^2 = \int_{R_i}^{R_o} r\,dr\left[\left(\nabla_r^2 - \frac{m^2}{r^2}\right)^2 f\right]\delta f + r\left[\left(\nabla_r^2 - \frac{m^2}{r^2}\right)f\right]\frac{d\delta f}{dr}\bigg|_{R_i}^{R_o} - r\frac{d}{dr}\left[\left(\nabla_r^2 - \frac{m^2}{r^2}\right)f\right]\delta f\bigg|_{R_i}^{R_o}.$$

For the second term, which is a boundary term, we obtain

$$\delta\kappa = \delta\frac{1}{2}\left[\left(\frac{df}{dr}\right)^2 - m^2\frac{d}{dr}\left(\frac{f^2}{r}\right)\right] = \left[\frac{df}{dr} - m^2\frac{f}{r}\right]\frac{d\delta f}{dr} - m^2\frac{d}{dr}\left(\frac{f}{r}\right)\delta f.$$

Therefore, the variation of the bending energy is

$$\delta U_B = \frac{2\pi}{2}B\int_{R_i}^{R_o} r\,dr\left[\left(\nabla_r^2 - \frac{m^2}{r^2}\right)^2 f\right]\delta f + \frac{2\pi}{2}B\left\{r\left[\left(\nabla_r^2 - \frac{m^2}{r^2}\right)f\right] - (1-\nu)\left(\frac{df}{dr} - m^2\frac{f}{r}\right)\right\}\frac{d\delta f}{dr}\bigg|_{R_i}^{R_o}$$

$$+ \frac{2\pi}{2}B\left\{-r\frac{d}{dr}\left[\left(\nabla_r^2 - \frac{m^2}{r^2}\right)f\right] + (1-\nu)m^2\frac{d}{dr}\left(\frac{f}{r}\right)\right\}\delta f\bigg|_{R_i}^{R_o}. \tag{C4}$$

b. Stretching energy

The first variation of the stretching energy gives the simple expression [after using the stress-strain relations and Eqs. (C3)]

$$\delta U_S = 2\pi \int_{R_i}^{R_o} r\,dr\,(\sigma_{rr}\,\delta\varepsilon_{rr} + \sigma_{\theta\theta}\,\delta\varepsilon_{\theta\theta} + 2\sigma_{r\theta}\,\delta\varepsilon_{r\theta}),$$

where we have included only the axisymmetric part of the strains (the super-index is henceforth dropped). The variations of the strains are

$$\delta\varepsilon_{rr} = \frac{d\delta u_r}{dr} + \frac{1}{2}\frac{df}{dr}\frac{d\delta f}{dr}, \quad \delta\varepsilon_{\theta\theta} = \frac{\delta u_r}{r} + \frac{m^2}{2r^2}f\delta f \quad \delta\varepsilon_{r\theta} = \frac{1}{2}\frac{d\delta u_\theta}{dr} - \frac{\delta u_\theta}{2r}.$$

Substituting the variations of the strains into the energy, we obtain after an integration by parts

$$\delta U_S = 2\pi \int_{R_i}^{R_o} dr \left\{ \left[\sigma_{\theta\theta} - \frac{d}{dr}(r\sigma_{rr})\right]\delta u_r - \left[\frac{d(r\sigma_{r\theta})}{dr} + \sigma_{r\theta}\right]\delta u_\theta + \left[\sigma_{\theta\theta}\frac{m^2}{2r}f - \frac{d}{dr}\left(\sigma_{rr}\frac{r}{2}\frac{df}{dr}\right)\right]\delta f \right\}$$

$$+ 2\pi\sigma_{rr}r\delta u_r|_{R_i}^{R_o} + 2\pi\sigma_{r\theta}r\delta u_\theta|_{R_i}^{R_o} + 2\pi\sigma_{rr}\frac{r}{2}\frac{df}{dr}\delta f\Big|_{R_i}^{R_o}. \tag{C5}$$

c. External work and mechanical energy

It is straightforward to obtain the variation of the external work as

$$\delta W^e = 2\pi T_o R_o \delta u_r(R_o) - 2\pi T_i R_i \delta u_r(R_i). \tag{C6}$$

Thus, we now have an explicit expression for the variation of the mechanical energy:

$$\delta U_M = \delta U_B + \delta U_S - \delta W^e, \tag{C7}$$

where the individual terms are given by Eqs. (C4)–(C6).

5. Equations and boundary conditions

Since the variations δf, δu_r, and δu_θ are independent, the variation of the mechanical energy is zero when the following terms in Eq. (C7) are zero:

$$\sigma_{\theta\theta} - \frac{d}{dr}(r\sigma_{rr}) = 0, \quad \frac{1}{r}\frac{d(r\sigma_{r\theta})}{dr} + \frac{\sigma_{r\theta}}{r} = 0,$$

$$B\left[\left(\nabla_r^2 - \frac{m^2}{r^2}\right)^2 f\right] + \left[\sigma_{\theta\theta}\frac{m^2}{r^2}f - \frac{1}{r}\frac{d}{dr}\left(\sigma_{rr}\,r\frac{df}{dr}\right)\right] = 0.$$

Using the first equation to simplify the third equation, we obtain

$$0 = \frac{1}{r}\frac{d(r\sigma_{r\theta})}{dr} + \frac{\sigma_{r\theta}}{r}, \tag{C8a}$$

$$0 = \frac{1}{r}\frac{d(r\sigma_{rr})}{dr} - \frac{\sigma_{\theta\theta}}{r}, \tag{C8b}$$

$$B\left(\nabla_r^2 - \frac{m^2}{r^2}\right)^2 f = \sigma_{rr}\frac{d^2 f}{dr^2} + \sigma_{\theta\theta}\left(\frac{1}{r}\frac{d}{dr} - \frac{m^2}{r^2}\right)f. \tag{C8c}$$

Thus, we have reobtained Eqs. (B3a) and (B3b) of Appendix B, showing that the minimization of the mechanical energy U_M yields these equations.

For the first variation of the mechanical energy to be zero, the boundary terms must also vanish. This requirement gives the boundary conditions necessary to solve the equations. In order for the boundaries to be subjected to constant stresses, the edge must be free and the values of δf, $d\delta f/dr$, δu_r, and δu_θ cannot be fixed there. That the boundary terms vanish yields the boundary conditions:

$$\sigma_{r\theta}|_{R_o} = 0, \quad \sigma_{r\theta}|_{R_i} = 0, \tag{C9a}$$

$$\sigma_{rr}|_{R_o} = T_o, \quad \sigma_{rr}|_{R_i} = T_i, \tag{C9b}$$

$$\left\{ r\left[\left(\nabla_r^2 - \frac{m^2}{r^2}\right)f\right] - (1-\nu)\left(\frac{df}{dr} - m^2\frac{f}{r}\right)\right\}\Big|_{R_i, R_o} = 0, \tag{C9c}$$

$$\left\{ B\left[-r\frac{d}{dr}\left[\left(\nabla_r^2 - \frac{m^2}{r^2}\right)f\right] + (1-\nu)m^2\frac{d}{dr}\left(\frac{f}{r}\right)\right] + r\sigma_{rr}\frac{df}{dr}\right\}\Big|_{R_i, R_o} = 0. \tag{C9d}$$

Equations (C9) correspond to the BCs (B4) derived in Appendix B. As before, the solution of the equilibrium equation (C8a) with the boundary condition (C9a) shows that $\sigma_{r\theta} = 0$.

APPENDIX D: THE SINGLE MODE AS A MINIMIZER OF THE ENERGY

Near the wrinkling threshold $\tau_c(\epsilon)$, there exists a single unstable mode with $m_c(\epsilon)$ wrinkles, and hence the pattern is exactly characterized by this single mode. However, as the system moves farther from threshold, more and more modes will become unstable. One might expect that the shape of the sheet takes the form

$$\zeta(r,\theta) = \sum f_m(r)\cos(m\theta), \tag{D1}$$

where the sum is over all unstable modes m. Here we present a heuristic argument for why this is not the case. Instead, the system, absent any adverse boundary conditions, will exhibit a single-mode shape in the FFT limit as well.

In the FFT limit, the energy can be written as the sum of two parts: a dominant energy U^{dom} that depends only on the external tensions and remains finite as $\epsilon \to 0$, and a subdominant energy U^{sub} that depends on the shape ζ and vanishes with ϵ [5]. The subdominant energy gets contributions both from the bending energy and from stretching terms associated with

out-of-plane deformations. The bending energy is quadratic in ζ (C1). The largest subdominant stretching terms come from the in-plane stress times the out-of-plane contributions to the strain (C2). These strain terms are also quadratic in ζ (C3), so the leading term in the subdominant energy will be proportional to ζ^2.

Though there is some r dependence in the energy, it is not strong. Barring a boundary condition that breaks the r symmetry, we expect that each mode should have roughly the same r dependence. That is, we should be able to write $f_m(r) = A_m g(r)$ for some universal function $g(r)$. Since the subdominant energy is quadratic in ζ, we may write

$$U^{sub} \approx \sum_{m=1}^{n} V_m A_m^2. \tag{D2}$$

The angular integral of the subdominant energy density causes the cross-terms between different modes to vanish. Our numerical results suggest that $g(r)$ is square integrable, so the radial integral will be well defined and establish the V_m. (For later ease of discussion, we consider only a finite number of modes n. But n may be taken to be infinite without altering the argument.) In this approximation, we can write $\sigma_{\theta\theta} = 0$, or equivalently, the slaving condition (3) schematically as

$$\sum_{m=1}^{n} C_m A_m^2 = C_0. \tag{D3}$$

We may use this expression to eliminate one amplitude from Eq. (D2). We choose to eliminate A_1^2 and rewrite the energy in terms of the remaining modes:

$$U^{sub} \approx U_1 + \sum_{m=2}^{n} \widetilde{V}_m A_m^2. \tag{D4}$$

Since U^{sub} is linear in the A_m^2, its minimization is an instance of linear programming. To put it in more familiar form, let $\mathbf{x} = (A_2^2, A_3^2, \ldots, A_n^2)$. Then the energy (D4) may be written as

$$U^{sub} - U_1 \approx \widetilde{\mathbf{V}}^T \mathbf{x}, \tag{D5}$$

where $\widetilde{\mathbf{V}} \equiv (\widetilde{V}_2, \ldots, \widetilde{V}_n)$. Because $A_m^2 \geqslant 0$, we have:

$$\mathbf{x} \geqslant 0, \quad \mathbf{C}^T \mathbf{x} \leqslant C_0, \tag{D6}$$

with $\mathbf{C} \equiv (C_2, \ldots, C_n)$, where the latter comes from the constraint (D3) and $A_1^2 \geqslant 0$. A basic result of linear programming is that the minimum to (D5) will occur at one of the corners of the domain defined by (D6) [24,25]. As $\mathbf{x} \in \mathbb{R}^{n-1}$, a corner of this domain must lie on $(n-1)$ equalities of (D6). Since each equality corresponds to one of the $A_m = 0$, this means $(n-1)$ of the n modes must vanish at the minimum energy, leaving a shape consisting of only a single mode.

The argument relies on all the modes having the same r dependence, so that the subdominant energy can be approximated by the form (D2). The consistency of the computed profiles (Fig. 3) suggests that it is not an unreasonable assumption. Note that near the end of the wrinkles, the profiles have different r dependencies. This indicates the failure of the slaving condition due to a compressional boundary layer. Whether this compressional layer leads to a failure of the argument that suggests a single-mode energy minimizer is an open question that has to be addressed in the future (see also Ref. [16]). Near $r = R_i$, on the other hand, the agreement of the profiles indicates that the free boundary conditions are nearly compatible with the single mode solution. Other boundary conditions may not be. For example, clamping $[f(R_i) = 0]$ induces compression and is obviously inconsistent with the slaving condition. In such a case, it is natural to expect the formation of modes with different dependencies on r. Because the above argument will still be valid away from the boundary, we expect a boundary layer in which multiple modes transit to the single optimal mode. This boundary layer, which occurs under strong radial tension, may develop to a cascade structure [26].

[1] S. P. Timoshenko and J. N. Goodier, *Theory of Elasticity* (McGraw Hill, New York, 1961).

[2] H. Wagner, Z. Flug. Motor. **20**, 8 (1929).

[3] E. H. Mansfield, *The Bending and Stretching of Plates* (Cambridge University Press, Cambridge, 1989).

[4] A. C. Pipkin, IMA J. App. Math. **36**, 85 (1986).

[5] B. Davidovitch, R. D. Schroll, D. Vella, M. Adda-Bedia, and E. Cerda, Proc. Nat. Acad. Sci. USA **108**, 18227 (2011).

[6] J. C. Geminard, R. Bernal, and F. Melo, Eur. Phys. J. E **15**, 117 (2004).

[7] J. Huang *et al.*, Science **317**, 650 (2007).

[8] D. P. Holmes and A. J. Crosby, Phys. Rev. Lett. **105**, 038303 (2010).

[9] H. King, R. D. Schroll, B. Davidovitch, and N. Menon, Proc. Nat. Acad. USA (to be published).

[10] D. Vella, M. Adda-Bedia, and E. Cerda, Soft Matter **6**, 5778 (2010).

[11] M. Stein and J. M. Hedgepeth, NASA Technical Note D-813 (1961).

[12] E. Cerda, K. Ravi-Chandar, and L. Mahadevan, Nature (London) **419**, 579 (2002).

[13] E. Cerda and L. Mahadevan, Phys. Rev. Lett. **90**, 074302 (2003).

[14] C. P. Coman and A. P. Bassom, J. Mech. Phys. Solids **55**, 1601 (2007).

[15] M. C. Cross and G. Greenside, *Pattern Formation and Dynamics in Nonequilibrium Systems* (Cambridge University Press, Cambridge, 2009).

[16] P. Bella and R. V. Kohn, arXiv:1202.3160.

[17] L. D. Landau and E. M. Lifshitz, *Theory of Elasticity* (Butterworth-Heinemann, Oxford, 1998).

[18] S. P. Timoshenko and J. M. Gere, *Theory of Elastic Stability* (McGraw Hill, New York, 1961).

[19] Notice that the Fourier integration $\int_0^{2\pi} d\theta \sin(3m\theta)(\cdot)$ of the normal force balance, Eq. (A2c), yields a fifth equation, that seems to overdetermine the set of equations (A9) for the four

functions. However, the mathematical procedure of Fourier decomposition outlined in Appendix A is still well defined, since there are higher modes in the stresses and strains that also contribute to the Fourier integration $\int_0^{2\pi} d\theta \sin(3m\theta)(\cdot)$ and have not been included in Eqs. (A8). Hence, the next equations in the hierarchy determine these higher modes.

[20] Note that the assumption $d/dr \sim 1/R_i$, which underlies this scaling analysis, is not valid under NT conditions, where the length ℓ of wrinkles (the characteristic scale for radial variation) vanishes as $\epsilon \to 0$. In the high bendability NT regime one finds $\ell/R_{in} \sim m^{-2/3} \ll 1$ [5], and hence we estimate $d/dr \sim 1/\ell \sim m^{2/3}/R_{in}$. Repeating the force balance of Eq. (A9d), we find $\sigma_{r\theta}^{(2m)} \sim m(\ell/R_{in})\sigma_{\theta\theta}^{(2m)}$ and $m\sigma_{r\theta}^{(2m)} \sim m^2(\ell/R_{in})\sigma_{\theta\theta}^{(2m)} \gg \sigma_{\theta\theta}^{(2m)}$. Substituting these expressions in Eq. (A9c) we conclude that the balance is

$$\frac{1}{\ell^2}\sigma_{rr}^{(2m)} \sim \frac{m}{R_{in}\ell}\sigma_{r\theta}^{(2m)} \sim \frac{m^2}{R_{in}^2}\sigma_{\theta\theta}^{(2m)},$$

which shows again, after estimating $df/dr \sim f/\ell$, that the three terms proportional to $\sigma_{rr}^{(2m)}$, $\sigma_{r\theta}^{(2m)}$, and $\sigma_{\theta\theta}^{(2m)}$ in Eq. (A9a) are of the same order.

[21] Again, this derivation does not apply in the NT regime, where the strain $(df/dr)^2$ is estimated as $(f/\ell)^2$ rather than $(f/R_i)^2$. However, the amplitude $f(r)$ vanishes in the NT limit, so $\sigma_{rr}^{(2m)} \propto f^2 \to 0$ is quite obviously much less than $\sigma_{rr}^{(0)}$. Here, too, $m \sim \epsilon^{-3/8} \gg 1$ for $\epsilon \ll 1$.

[22] D. J. Struik, *Lectures on Classical Differential Geometry* (Dover, New York, 1988).

[23] Note that the full form of the strain-displacement relations (A6)–(A7) must be used, instead of the reduced form (C3).

[24] W. H. Press, B. P. Flannery, S. A. Teukolsky, and W. T. Vetterling, *Numerical Recipes in C* (Cambridge University Press, Cambridge, 1992).

[25] It is possible for the minimum to appear at several corners, and therefore also on the subspace spanning them. Such degenerate cases form a set of measure zero in the parameter space, so we do not deal with them.

[26] R. D. Schroll, E. Katifori, and B. Davidovitch, Phys. Rev. Lett. **106**, 074301 (2011); B. Davidovitch, Phys. Rev. E **80**, 025202(R) (2009).